



HiSOR



ACTIVITY REPORT

2019

**Hiroshima Synchrotron Radiation Center, HiSOR
Hiroshima University**

HiSOR ACTIVITY REPORT

2019

Hiroshima Synchrotron Radiation Center, HiSOR

Hiroshima University

Edited by Y. Izumi

The annual report is available from

Hiroshima Synchrotron Radiation Center, Hiroshima University
Kagamiyama 2-313, Higashi-Hiroshima 739-0046, JAPAN

Phone: +81-82-424-6293

Fax: +81-82-424-6294

e-mail: hisor@hiroshima-u.ac.jp

URL: <http://www.hsrc.hiroshima-u.ac.jp/>

Preface

The Hiroshima Synchrotron Radiation Center was inaugurated in 1996, as part of the academic policies of the Ministry of Education, Culture, Sports, Science and Technology (MEXT), Japan. A compact 700MeV electron-storage ring, called HiSOR (this center is often referred as HiSOR), produces synchrotron radiation in the range of ultraviolet and soft x-ray range. The mission of HiSOR is to promote advanced research in the field of condensed matter physics including interdisciplinary fields using synchrotron radiation, as well as to develop human resources making the most of the international research environment established inside the national university. HiSOR has been authorized as a “Joint Usage / Research Center” by the MEXT since FY2010.

In FY2019, Dr. Shunya Matsuba has moved to JASRI/SPring-8, and Dr. Koji Miyamoto has been promoted to Associate Professor of HiSOR. Prof. Masahiro Katoh has arrived at HiSOR from UVSOR, and Dr. Miho Shimada has arrived from KEK on cross appointment, which further strengthen collaborations among HiSOR, UVSOR, and KEK, including the development of a compact storage ring suitable for HiSOR II.

As concerns the joint usage/research activities of FY2019, we have accepted 238 users (real number) in total; 79 users from Hiroshima University, 95 users from domestic institutes, 64 users from foreign institutes. We have accepted 130 proposals; 44 proposals from Hiroshima University, 43 proposals from inside Japan, and 43 proposals from outside Japan. Detailed scientific results are reported in this volume. We have published 42 papers in 2019, and 24 papers (57% of total number) have been written through international collaborations. The number of top 10% paper is 6 which is 14% of total number, indicating quality of the research.

From Oct. 20 to Nov. 2, 2019, Dr. Eike F. Schwier from HiSOR and Dr. Yasmine Sassa from Chalmers University of Technology organized MIRAI PhD School 2019, “Electronic and Magnetic Properties of Materials Using Large Scale Facilities”, in collaboration with J-Parc. The program consists of lectures, group work sessions, poster presentations and hands-on experiments at HiSOR and J-Parc. Students and postdoctoral fellows (7 from Japanese and 12 from Swedish universities) from various fields participated this program.

Due to the pandemic of new corona virus it was unfortunate that our international users could not come since early 2020, and we should cancel the 24th Hiroshima International Symposium on Synchrotron Radiation. We really hope the situation will be better in the near future and restart collaborative projects with outside researchers as before.

In closing, I would like to thank all the staff members for their great efforts to operate HiSOR, and to maintain and advance experimental stations. I also want to thank our students and collaborators for their excellent scientific achievements, making full use of our facilities. Finally, I deeply appreciate the continued supports by Hiroshima University and the MEXT.



July 2020

Kenya Shimada

Kenya Shimada

Director of Hiroshima Synchrotron Radiation Center

Table of Contents

Preface

Current Status of HiSOR

Status of the HiSOR storage ring.....	1
Beamlines	5

Research Activities

—Accelerator Studies—

Study on temporal structures of synchrotron radiation by using interferometer	8
S. Notsu, S. Matsuba, K. Kawase, M. Katoh	
Design study on laser focusing system for 90 degree Thomson scattering gamma-ray source.....	10
H. Kunimune, Y. Okano, M. Katoh	
Simulation study on beam injection to compact synchrotron using pulse octupole magnet.....	12
K. Hirata, T. Ishida, M. Shimada, M. Katoh	

—Synchrotron Radiation Experiments—

Study of electronic state of oxygen adsorbed Nb(110) using high-resolution angle-resolved photoemission spectroscopy.....	14
Y. Miyai, E. F. Schwier, K. Shimada	
High-resolution polarization-dependent angle-resolved photoemission spectroscopy study of O-Fe(100) thin films grown on MgO(100)	16
M. Zheng, E. F. Schwier, K. Shimada	
Electrical structure and H-T phase diagram of $\text{Eu}(\text{Fe}_{1-x}\text{Rh}_x)_2\text{As}_2$	19
S. Xiao, D. C. Peets, Y. Feng, W. -H. Jiao, E. F. Schwier, K. Shimada, S. He	
Direct band structure study of magnetic Weyl semimetal candidate V_3S_4 using ARPES	22
X. -M. Ma, Y. -J. Hao, Y. Feng, C. Zhou, C. Liu	
Observation of topological surface state in palladium-bismuth superconductor.....	24
M. Sakano, Y. Kubota, K. Okawa, K. Sumida, E. F. Schwier, K. Shimada, T. Okuda, T. Sasagawa, K. Ishizaka	
Band structures of cubic PtBi_2 studied by ARPES	26
Y. Feng, S. He, S. Xiao, B. Feng	

Changing band alignment with adsorbed palladium on MoS ₂ and WSe ₂	28
T. Komesu, E. F. Schwier, P. E. Evans, S. Kumar, K. Shimada, P. A. Dowben	
Resonance photoemission study of the energy gap open at the Dirac point and the reasons of the gap formation in Gd-doped magnetic topological insulators	30
D. A. Estyunin, A. M. Shikin, E. F. Schwier, S. Kumar, A. Kimura	
Exchange vs. spin-orbit interaction at magnet/heavy-metal interfaces	32
M. Holtmann, P. J. Grenz, S. Kumar, E. F. Schwier, K. Miyamoto, T. Okuda, M. Donath	
Angle-resolved photoelectron spectroscopy study of (Ce,La)Ru ₂ Al ₁₀	34
H. Yamaoka, H. Tanida, E. F. Schwier, S. Kumar, M. Arita, K. Shimada	
Electronic structure of elementary excitation in quantum spin liquid.....	36
C. Liu, Y. Wang, L. –L. Huang, X. –M. Ma, Y. –J. Hao, K. Deng, C. Liu, Z. –Y. Hao, E. F. Schwier, S. Kumar, H. Sato, K. Shimada, L. Wang, J. Mei, C. Chen	
Experimental evidence of monolayer AlB ₂ with symmetry-protected Dirac cones	38
D. Geng, K. Yu, S. Yue, J. Cao, W. Li, D. Ma, C. Cui, M. Arita, S. Kumar, E. F. Schwier, K. Shimada, P. Cheng, L. Chen, K. Wu, Y. Yao, B. Feng	
ARPES study of a new type-II Dirac semimetal candidate NiTe ₂	42
S. Xiao, Y. Feng, E. F. Schwier, K. Shimada, S. He	
ARPES study on Zintl phase Ba ₃ Cd ₂ As ₄ – A proposed topological crystalline insulator protected by C ₂ rotational symmetry	44
X. –M. Ma, Y. –J. Hao, Y. Feng, N. Ni, C. Liu	
ARPES measurements on thin films of topological crystalline insulator Pb _x Sn _{1-x} Te .	46
T. Watanabe, T. Shimano, Y. Tomohiro, K. Hiwatari, R. Akiyama, S. Kumar, A. Kimura, K. Shimada, S. Hasegawa, S. Kuroda	
ARPES study of type-II nodal loop in trigonal layered PtBi ₂	48
S. Xiao, Y. Feng, X. Wu, E. F. Schwier, M. Arita, K. Shimada, S. He	
Evidence of a bulk band structure for SrIrO ₃ thin films	50
T. Komesu, S. Kumar, P. E. Evans, A. J. Yost, E. F. Schwier, K. Shimada, L. Zhang, X. Hong, P. A. Dowben	
High-resolution ARPES and pressure dependent magneto-transport study of BiSbTe ₃	52
V. K. Gangwar, S. Kumar, M. Singh, L. Ghosh, Z. Yufeng, Y. Kumar, P. Shahi, S. Patil, E. F. Schwier, K. Shimada, Y. Uwatoko, A. K. Ghosh, S. Chatterjee	
Ex-situ/in-situ soft x-ray absorption investigation towards passivation behavior of Ti	54
Y. Jin, Q. Wang, F. –F. Huang, Y. –T. Cui, H. Yoshida, T. Tokushima	

X-ray absorption spectroscopy of single layer graphene on metal supports	56
M. Kato, K. Nishiyama, S. Oka, S. Yasuda, S. Wada, H. Yoshida, I. Yagi	
Soft X-ray absorption spectra of copper ion complexes included in cyclodextrin.....	57
Y. Nakamura, R. Nobue, H. Yoshida	
Electronic structures of Mg-Zn-Gd alloys with long-periodic stacking order.....	58
S. Hosokawa, J. R. Stellhorn, K. Kobayashi, K. Maruyama, H. Sato	
Direct observation of electronic structure of cycloparaphenylenes.....	60
K. Kanai	
Electronic structures of Mn-based oxypnictides studied by photoemission spectroscopy	62
A. Higashiya, K. Nakagawa, M. Arita, H. Sato, K. Takase, A. Yamasaki	
Direct observation of unoccupied and occupied electronic structure of cycloparaphenylenes.....	64
K. Kanai	
The observation of the composition dependence of the electronic structure in half-metal Heusler alloy $\text{Co}_2\text{Fe}(\text{Ga}_x\text{Ge}_{1-x})$	66
K. Goto, Y. Sakuraba, T. Kono, H. Sato, K. Hono	
Photoelectron spectroscopy of Yb_4TGe_8 II.....	68
H. Yamaoka, S. Yamanaka, M. Hikiji, C. Michioka, N. Tsujii, H. Sato, K. Shimada, K. Yoshimura	
Electronic states of lipoic acid and related molecules included in cyclodextrin	70
K. Ando, K. Baba, H. Sato, H. Yoshida	
Photoemission study of the occupied molecular orbital in a TADF neat film.....	71
Y. Fukami, K. Fukumoto, H. Sato, Y. Yamada	
Characterization of graphene nanomesh fabricated on Cu (111) surface by surface reaction	73
Y. Nagatomo, H. Sakaue, Y. Tominari, S. Tanaka, H. Sato, H. Suzuki	
Surface-state Coulomb repulsion accelerates a metal-insulator transition in topological semimetal nanofilms	75
S. Ito, M. Arita, J. Haruyama, B. Feng, W. –C. Chen, H. Namatame, M. Taniguchi, C. –M. Cheng, G. Bian, S. –J. Tang, T. –C. Chiang, O. Sugino, F. Komori, I. Matsuda	
ARPES studies of the layered ternary superconductors with low-carrier-density.....	77
Y. Akimoto, K. Kuroda, K. Kawaguchi, Y. Arai, M. Arita, D. Hirai, Z. Hiroi, T. Yamada, T. Kondo	
Angle-resolved photoemission spectroscopy of valence transition compound YbInCu_4	79
K. Maeda, T. Matsumoto, Y. Tanaka, H. Sato, M. Arita, K. Shimada, K. Matsumoto, K. Hiraoka	

Three-dimensional band structure characteristics of the magnetic topological insulator MnBi_2Te_4	81
Y. –J. Hao, R. Lu, M. Arita, C. Liu, C. Chen	
High-resolution photoemission study of RuAs.....	83
D. Ootsuki, T. Ishida, Y. Yuzawa, M. Arita, D. Hirai, H. Takagi, T. Mizokawa, T. Yoshida	
ARPES study of non-uniform charge transfer and circular dichroism in vanadium intercalated NbS_2	85
M. Novak, X. –X. Wang, A. Kimura	
Photoemission study of mechanical polished SmB_6 [110] surface.....	86
M. Arita, H. Sato, K. Shimada, H. Namatame, M. Taniguchi, H. Tanida, Y. Osanai, K. Hayashi, F. Iga,	
Photon energy dependent ARPES study on magnetic topological insulators	
$\text{Mn}(\text{Bi}_{1-x}\text{Sb}_x)_2\text{Te}_4$	87
Y. –J. Hao, X. –M. Ma, K. Zhang, R. Lu, M. Zeng, X. –R. Liu, M. Arita, E. F. Schwier, S. Kumar, K. Shimada, C. Chen, C. Liu	
Radial spin texture in elemental tellurium with chiral crystal structure	89
M. Sakano, T. Takahashi, S. Akebi, M. Nakayama, K. Kuroda, K. Taguchi, T. Yoshikawa, K. Miyamoto, T. Okuda, N. Mitsuishi, K. Ishizaka, S. Shin, T. Sasagawa, T. Kondo	
Spin polarization study on single-spin Dirac cones in the magnetic kagome metal Fe_3Sn_2	91
X. –M. Ma, Y. Feng, C. Wang, Y. –J. Hao, T. –X. Han, H. –W. Shen, Y. –M. Xu, C. Liu	
Spin-resolved ARPES study on charge density wave material TaTe_2	93
M. Sakano, N. Mitsuishi, Y. Takahashi, T. Akiba, K. Miyamoto, T. Okuda, S. Ishiwata, K. Ishizaka	
Spin-resolved ARPES measurement on magnetic topological insulators MnBi_2Te_4 ..	95
Y. –J. Hao, K. Miyamoto, T. Okuda, C. Liu	
Synchrotron radiation spin-resolved ARPES study for thin film of half-metal Heusler compounds $\text{Co}_2\text{Fe}(\text{Ga}_{0.5}\text{Ge}_{0.5})$	97
K. Goto, Y. Sakuraba, M. Kakoki, T. Kono, T. Okuda, K. Hono	
Spin-resolved ARPES study on charge density wave material NbTe_2	99
M. Sakano, N. Mitsuishi, K. Miyamoto, T. Okuda, H. Takahashi, S. Ishiwata, K. Ishizaka	
ARPES study of In-doped (111) $\text{Pb}_x\text{Sn}_{1-x}\text{Te}$ close to band inversion compositions .	101
V. Golyashov, T. Okuda, A. Kimura, O. Tereshchenko	

Study of temperature-induced topological phase transition in TlBiS ₂ and TlBiSe ₂ ..	103
T. Imai, K. Kato, T. Matsuda, J. Chen, K. Miyamoto, A. Kimura, T. Okuda	
Performance evaluation of graphene coated Co (0001) / W (110) as a target of spin-detector for out-of-plane spin component and the observation of its electronic structure	105
Y. Baba, T. Okuda, K. Miyamoto	
Adsorption mechanism of hydrogen sulfide gas on granulated coal ash.....	107
S. Asaoka, H. Saito, T. Ichinari, T. Oikawa, S. Hayakawa	
Chemical composition of calcium species in fertilization pellets produced from anaerobic digestate.....	108
S. Asaoka, G. Yoshida, I. Ihara, S. Hayakawa	
Sulfur K-edge XAFS structural analysis of the acid decomposition reaction of diethyldithiocarbamate	110
A. Doi, J. R. Stellhorn, K. Komaguchi, S. Hayakawa	
Identification of sulfur species in marine sediments collected from the western part of Seto Island Sea, Japan.....	112
S. Asaoka, S. Hayakawa, K. Takeda	
Transmission curve measurement of the vacuum window installed in the X-ray astronomy satellite	114
T. Midooka, M. Tsujimoto, S. Kitamoto, S. Hayakawa	
Structure of a novel amorphous organic-inorganic hybrid tin cluster exhibiting nonlinear optical effects by low-energy XAFS measurements.....	116
J. R. Stellhorn, S. Hayakawa, B. Paulus, B. D. Klee	
Interaction mechanism between α_1 -acid glycoprotein and bio-membrane characterized by vacuum-ultraviolet circular-dichroism spectroscopy.....	117
K. Matsuo, M. Kumashiro, K. Gekko	
Electrostatic interaction between an N-terminal fragment of myelin basic protein and a phosphatidylinositol membrane characterized by synchrotron radiation circular dichroism spectroscopy	118
M. Kumashiro, Y. Izumi, K. Matsuo	
Optical activity measurement of amino acid films by circular dichroism spectroscopy	120
J. Takahashi, T. Sakamoto, Y. Izumi, K. Matsuo, M. Fujimoto, M. Katoh, Y. Kebukawa, K. Kobayashi	
Structure analysis of dimer and multimer of DNA repair protein, XRCC4, using VUV-CD.....	122
K. Nishikubo, M. Hasegawa, Y. Izumi, K. Fujii, K. Matsuo, Y. Matsumoto, A. Yokoya	

Determination of the degree of linear polarization in BL-13 by using a planarly-oriented material	124
M. Tabuse, K. Yamamoto, S. Wada	
XANES and XPS measurements of Br-incorporated DNA related molecules.....	126
M. Hirato, K. Fujii, S. Wada, Y. Baba, A. Yokoya	
X-ray absorption spectroscopy and photoelectron spectroscopy for a deliquescent ionic liquid.....	127
Y. Hikosaka, S. Wada	
Valence trends in $\text{Sm}(\text{Co}_{1-x}\text{Cu}_x)_5$ and $\text{Ce}(\text{Cu}_{1-x}\text{Co}_x)_5$	129
T. Ueno, H. Shishido, K. Saito, M. Sawada, M. Matsumoto	
Magnetic property of nickel hydroxide nanosheet	131
Y. Naruo, S. Uechi, M. Sawada, A. Funatsu, F. Shimojo, S. Ida, M. Hara	
Magnetic study of Co/h-BN/Fe/Ni interface by soft X-ray magnetic circular dichroism	133
T. Mayumi, Y. Ohashi, M. Sawada	
Hydrogen effects on the magnetic property of Laves phase GdCo_2 probed by XMCD	134
S. Kanamori, K. Ishimoto, N. Ishimatsu, N. Kawamura, K. Sakaki, M. Sawada, Y. Nakamura, S. Nakano	
Development of a measurement software for soft X-ray reflectometry with high usability and flexibility in axes control	136
K. Machida, T. Mayumi, M. Sawada	
High quality Cr_2O_3 layers growth on graphene-covered Ni(111) substrate.....	137
X. Hou, M. Sawada	

—Off-line Experiments—

Temperature dependent study of the Dirac point energy gap in magnetic stoichiometric topological insulators MnBi_2Te_4	138
D. A. Estyunin, I. I. Klimovskikh, A. M. Shikin, A. Kimura, S. Kumar, E. F. Schvier	
Study of the Dirac point energy gap in various magnetically doped topological insulators.....	140
D. A. Estyunin, A. M. Shikin, A. A. Rybkina, I. I. Klimovskikh, A. Kimura, S. Kumar, E. F. Schvier	
ARPES studies of the polarization-dependent features of the electronic structure of ultrathin ferromagnetic films grown on the PST and BSTS topological insulators for spintronic applications	142
A. K. Kaveev, O. E. Tereshchenko, V. A. Golyashov, E. F. Schvier	

Micro-ARPES study of topological material Ag-doped Bi_2Se_3	144
R. Eguchi, E. F. Schwier, L. Zhi, T. Taguchi, K. Kobayashi, H. Goto, Y. Kubozono	
High resolution laser-ARPES study on magnetic topological insulators MnBi_4Te_7 .	146
X. –M. Ma, Y. –J. Hao, Y. Feng, M. Zeng, Z. Hao, Y. Wang, S. Kumar, E. F. Schwier, K. Shimada, C. Chen, C. Liu	
ARPES study on in-plane antiferromagnetic axion insulator candidate EuIn_2As_2	148
Y. Zhang, K. Deng, X. Zhang, M. Wang, Y. Wang, C. Liu, J. –W. Mei, S. Kumar, E. F. Schwier, K. Shimada, C. Chen, B. Shen	
Electronic band structure study on the surfaces of magnetic topological insulators $\text{MnBi}_6\text{Te}_{10}$	150
X. –M. Ma, Z. Chen, E. F. Schwier, Y. –J. Hao, R. Lu, Y. Jin, M. Zeng, X. –R. Liu, Z. Hao, K. Zhang, W. Mansuer, S. Kumar, Y. Wang, C. Liu, K. Deng, J. Mei, K. Shimada, W. Huang, C. Liu, H. Xu, C. Chen	
Instabilities and their competition in doped or intercalated VSe_2	152
C. S. Yadav, E. F. Schwier, A. Taraphder	
Laser-photoemission spectroscopy on the magnetic topological insulators $\text{V}:(\text{Bi},\text{Sb})_2\text{Te}_3$ and MnBi_2Te_4	154
P. Kagerer, R. C. Vidal, C. I. Fornari, T. R. F. Peixoto, H. Bentmann, F. Reinert	

Appendices

Organization.....	157
List of publications	162
List of accepted research proposals	167
Symposium, Workshop, and HiSOR Seminar	175
Plan of the building.....	177
Location	178

Current Status of HiSOR

Status of the HiSOR storage ring

1. Introduction

The HiSOR is a synchrotron radiation (SR) source of Hiroshima Synchrotron Radiation Center, Hiroshima University, established in 1996. It is a compact racetrack-type storage ring having 21.95 m circumference, and its natural emittance of 400π nmrad is rather large compared with those of the other medium to large storage rings. The most outstanding advantage of the facility lies in good combination with state-of-the-art beamlines (BL's) for high-resolution photoelectron spectroscopy in the photon energy ranges between VUV and soft X-ray. The principal parameters of HiSOR are shown in Table 1.

HiSOR has two 180-deg. Normal-conducting bending magnets which generate a strong magnetic field of 2.7 T. This storage ring is equipped with two insertion devices, a linear undulator and a quasi-periodic APPLE-II undulator which replaced to the previous helical undulator in summer 2012. Major parameters of these undulators are listed in Table 2. The photon energy spectra of the SR from HiSOR are shown in Figure 1.

Table 1: Main parameters of the HiSOR Storage ring.

Circumference	21.95 m
Type	Racetrack
Bending radius	0.87 m
Beam energy at Injection	150 MeV
at Storage	700 MeV
Magnetic field at Injection	0.6 T
at Storage	2.7 T
Injector	150 MeV Racetrack Microtron
Betatron tune (ν_x, ν_y)	(1.72, 1.84)
RF frequency	191.244 MHz
Harmonic number	14
RF voltage	200 kV
Stored current (nominal)	300 mA
Natural emittance	400π nmrad
Beam life time	~10 hours@200 mA
Critical wavelength	1.42 nm
Photon intensity (5 keV)	1.2×10^{11} /sec/mr ² /0.1% b.w./300mA

Table 2: Main parameters of the undulators.

Linear undulator (BL-1)	
Total length	2354.2 mm
Periodic length λu	57 mm
Periodic number	41
Pole gap	30-200 mm
Maximum magnetic field	0.41 T
Magnetic material	Nd-Fe-B (NEOMAX-44H)
Quasi-Periodic APPLE-II undulator (BL-9A,B)	
Total length	1845 mm
Periodic length λu	78 mm
Periodic number	23
Pole gap	23-200 mm
Maximum magnetic field	0.86 T (horizontal linear mode) 0.59 T (vertical linear mode) 0.50 T (helical mode)
Magnetic material	Nd-Fe-B (NEOMAX-46H)

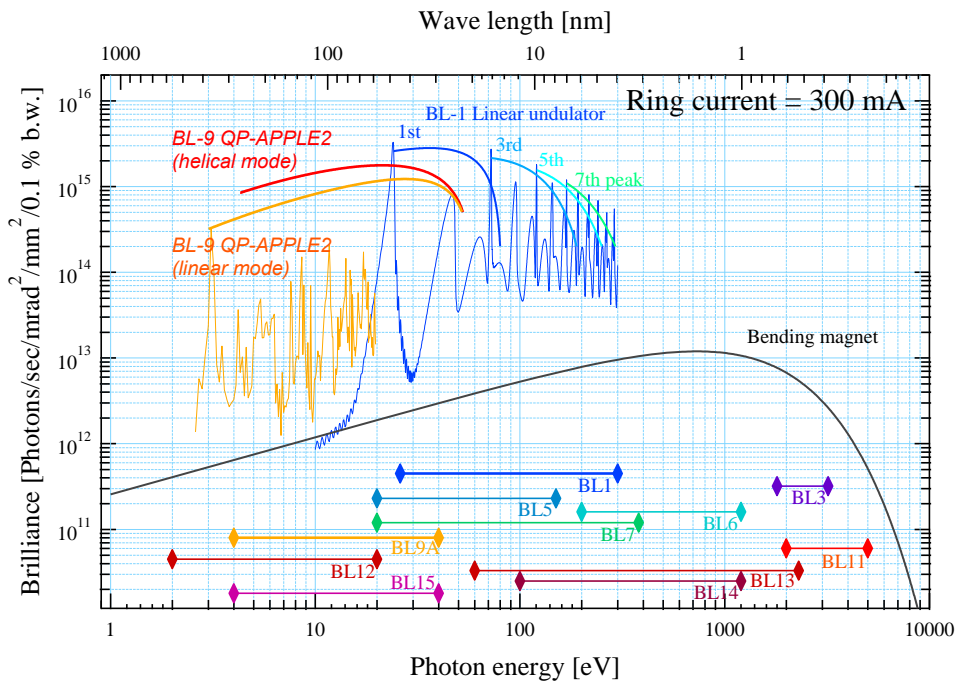


Figure 1: Photon energy spectra of the SR from HiSOR.

2. Operation status in FY 2019

The ring is operated for users from Tuesday to Friday. Figure 2 shows an example of typical users operation for one day. Beam injection for HiSOR is executed twice a day, at around 9:00 and 14:30. Machine is operated for machine conditionings and studies on Monday.

Figure 3 shows monthly operation time of HiSOR storage ring in FY 2019. HiSOR has a long term shutdown period for maintenance works in every summer. The total user time of FY2019 achieved 1660 hours. After the vacuum troubles at the storage ring in 2014 and 2015, the operation time has been recovered and is slightly increasing.

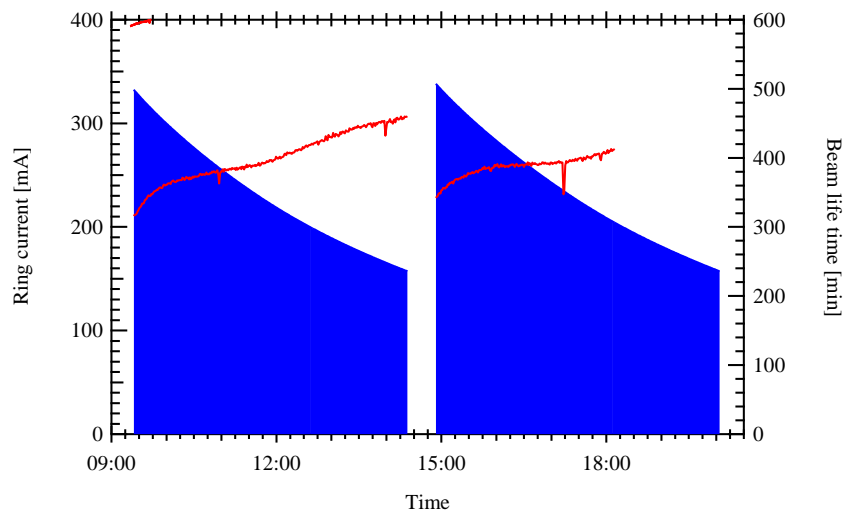


Figure 2: Typical daily operation status.

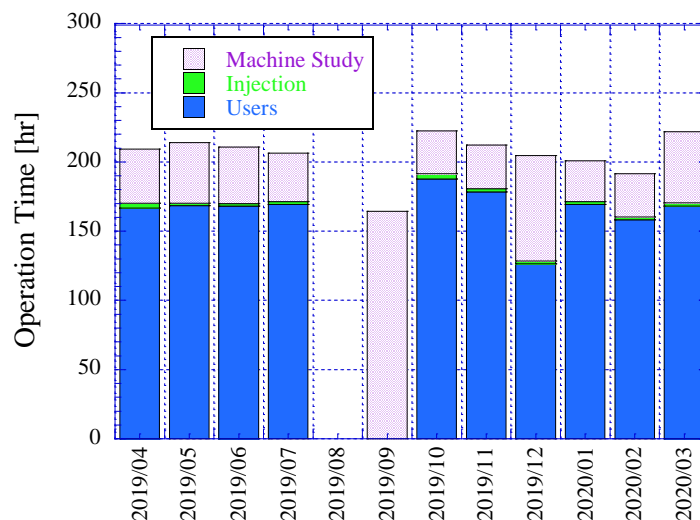


Figure 3: Monthly operation time in FY 2019.

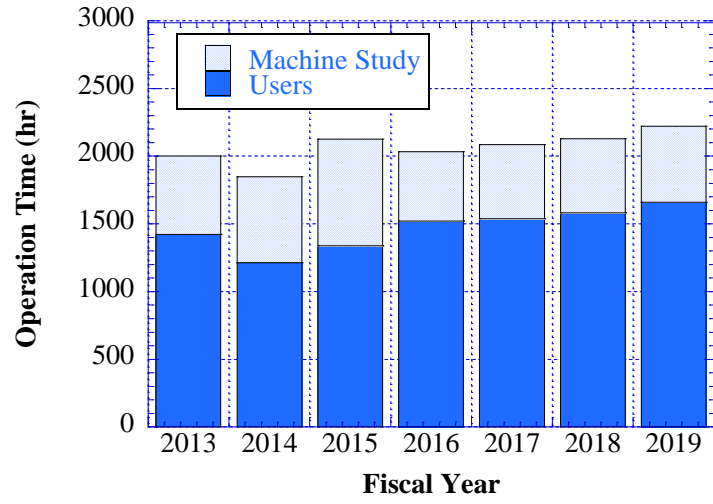


Figure 4: Operation time in FY 2013-2019.

Beamlines

A total of 13 beamlines has been constructed so far; three normal-incidence monochromators, seven grazing-incidence monochromators, two double crystal monochromators and apparatus for white beam irradiation (Fig. 1). Table 1 lists the beamlines at present together with the main subject, energy range and monochromators.

Table 1: List of Beamlines

Beamline	Source	Monochromator	Subject	Energy range (eV)	Status
BL-1	LU	GIM	Polarization dependent high-resolution ARPES	22-300	In use
BL-3	BM	DCM	Surface XAFS	1800-3200	In use
BL-4	BM		White beam irradiation		Closed
BL-5	BM	GIM	ARPES and PEEM	40-220	In use
BL-6	BM	GIM	Gas-phase photochemistry	200-1200	In use
BL-7	BM	GIM	ARPES	20-380	In use
BL-8	BM		Beam diagnosis		In use
BL-9A	HU/LU	NIM		5-35	In use
BL-9B	HU/LU	GIM	High-resolution spin-resolved ARPES	16-300	In use
BL-11	BM	DCM	XAFS	2000-5000	In use
BL-12	BM	NIM	VUV-CD of biomaterials	2-10	In use
BL-13	BM	GIM	Surface photochemistry	60-1200	In use
BL-14	BM	GIM	Soft-XMCD of nano-materials	400-1200	In use
BL-15	BM	NIM	VUV-CD of biomaterials	4-40	Closed
BL-16	BM		Beam profile monitor		In use

At present, nine beamlines BL1, BL3, BL6, B7, BL9A, BL9B, BL11, BL12, BL13 and BL14 are opened for users. Furthermore, three offline systems, resonant inverse photoemission spectrometer (RIPES), low-temperature scanning tunneling microscope (LT-STM) system, high-resolution angle-resolved photoemission spectrometer using ultraviolet laser (Laser ARPES) are in operation (Fig. 2).

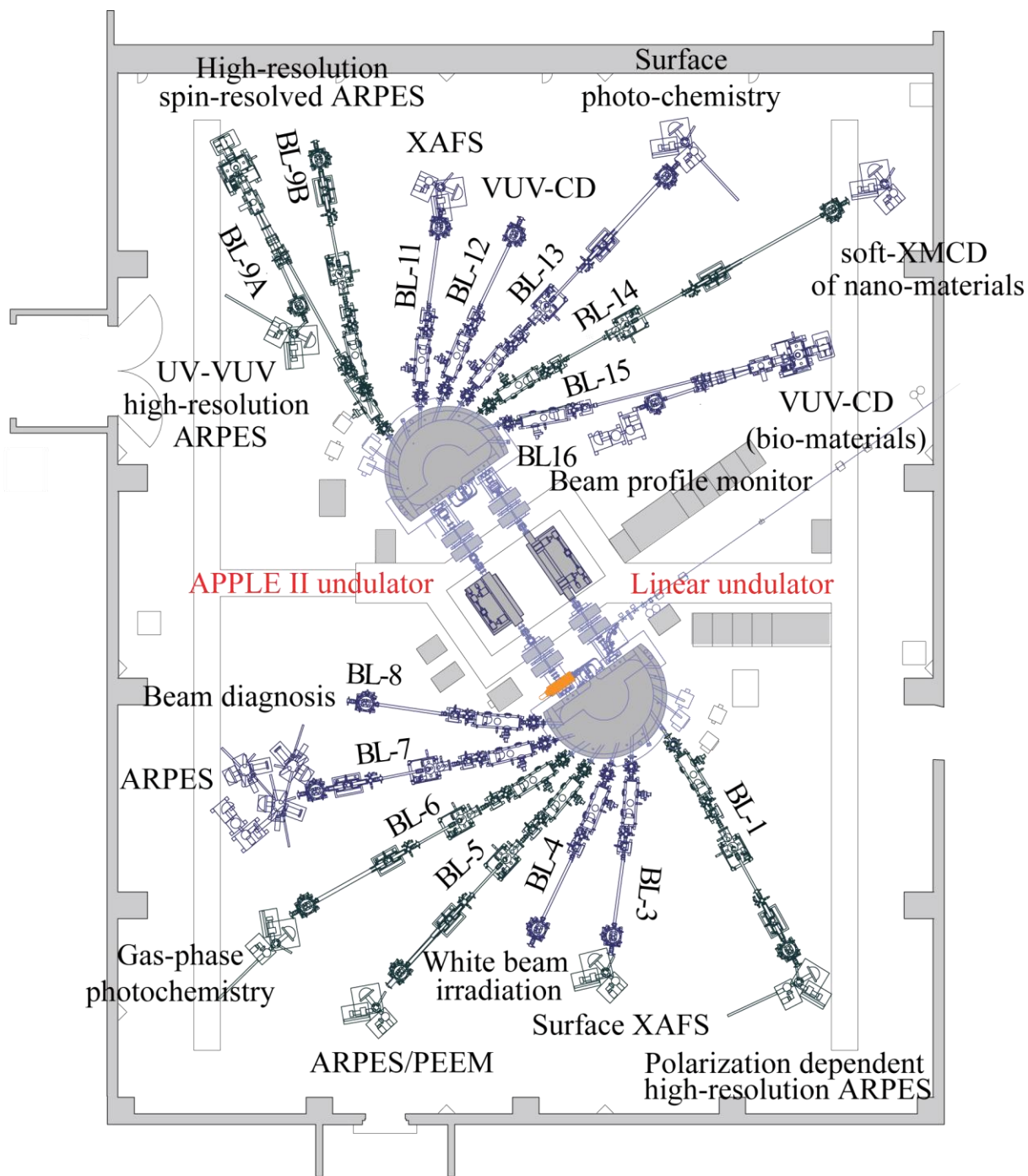


Fig. 1: Schematic view of the experimental hall.

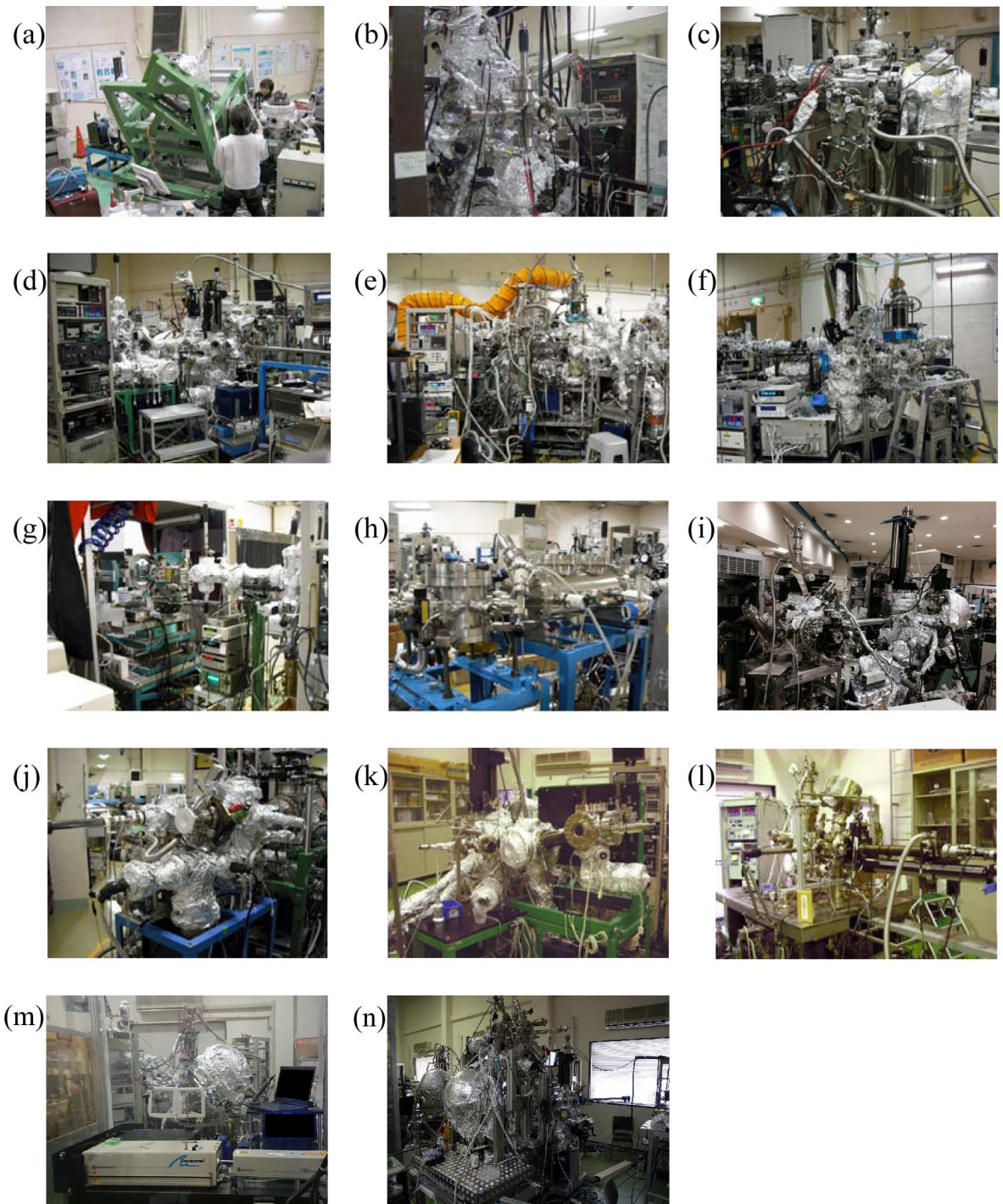


Fig. 2: Experimental stations on the beamline and offline: (a) BL-1, (b) BL-3, (c) BL-6, (d) BL-7, (e) BL-9A, (f) BL-9B, (g) BL-11, (h) BL-12, (i) BL-13, (j) BL-14, (k) RIPES (offline), (l) LT-STM (offline), (m) Laser ARPES (offline), (n) Laser spin-ARPES (offline).

Research Activities

– Accelerator Studies –

Study on Temporal Structure of Synchrotron Radiation by using Interferometer

Shohei Notsu^a, Syunya Matsuba^b, Keigo Kawase^c, Masahiro Katoh^{a,d}

^a Hiroshima University, 1-3-1 Kagamiyama, Higashi-Hiroshima 739-8526, Japan

^b Japan Synchrotron Radiation Research Institute (JASRI), 1-1-1, Kouto, Sayo-cho, Sayo-gun, Hyogo 679-5198 Japan

^c National Institutes for Quantum and Radiological Science and Technology (QST), 2-4 Shirakata, Tokai-mura, Naka-gun, Ibaraki 319-1106, Japan

^d Institute for Molecular Science, National Institutes of Natural Sciences, 38 Nishigo-Naka, Myodaiji, Okazaki, 444-8585, Japan

Keywords: Coherence. Undulator, Interferometer

Temporal structure of synchrotron radiation may be separated into two categories. The first one is the that of a photon wave packet emitted from a single electron. In case of the bending radiation, the wave packet forms a half cycle wave whose length is related to the critical photon energy. In case of undulator radiation, it forms a several-cycle wave whose cycle number is exactly same as that of the undulator magnetic period. Another temporal structure is the width of the light pulse emitted from a bunch of electrons, which comprises of many wave packets randomly distributing over the length of the electron bunch.

Usually the pulse length of synchrotron radiation, which is typically 10 to 100 psec, is measured with a streak camera. However, there is no report on the direct measurement of the wave packet length. In the laser field, it was demonstrated to measure both the light pulse width and the wave packet length (coherence length) by using an interferometer based on the photon correlation [1]. By using same method, it was demonstrated to measure the pulse width of the bending radiation [2].

In this study, we challenged to measure both the pulse width and the coherent length of the undulator radiation using an interferometer. A set of photomultiplier tubes were used for the photon detection. We constructed a high voltage power supply for them. They are tested at HiSOR-BL8. The result is shown in FIG. 1. The bunch filling of HiSOR was clearly measured and the result was consistent with the measurement by using a pickup electrode on the storage ring. It should be noted that the time resolution of the photomultiplier tubes is a few nsec and they are not capable of directly measuring the pulse width of the synchrotron radiation which is about 100 psec, however, in the photon correlation method, the temporal resolution is not limited by the detector resolution [2].

We constructed an interferometer as shown in FIG. 2, which is a modification of Michelson-type interferometer. The incoming synchrotron radiation is separated into two beams by a beam splitter and they go into corner-cube-mirrors and are reflected. Then, they go into another beam splitter and are merged. Finally, they go into two detectors. In this sense, the interferometer may be similar to Mach-Zehnder type in its function. One of the two corner-cube-mirrors is on a movable stage. We can change the path length of one of the separated beams.

Two experiments can be conducted on this interferometer. The first one is two-photon correlation and another is autocorrelation. In the former, the synchrotron radiation is reduced in its intensity by using pinholes and ND filters so that only a few photons are contained in a pulse. If two photons are incoming into the second splitter simultaneously, as can be shown based on the quantum mechanics, both of them should be detected by one of two detectors. Therefore, by moving one corner-cube-mirror, the coincidence rate of two photomultipliers is reduced when the two light pulses are temporally overlapped. From such observation, one can get information on the pulse length [1]. In the latter, each wave packet interferes with itself when the path lengths of the separated beams are exactly same. In this condition, one can observe a clear interference pattern by using a CCD camera. One can get information on the coherence length of the wave packets from the range of the path difference where the interference pattern appears.

We conducted a series of experiments by using an undulator beamline BL1U at UVSOR, IMS. We extracted the undulator radiation at a wavelength of 355 nm and introduced it to the interferometer. The details of the results will be presented in a future paper. Here, we only give a short summary. Concerning two-photon correlation, so far we could not get a significant result, which gives the information on the pulse length. On the other hand, in the autocorrelation experiment, we can get a clear result on the coherence length. Also, we note that the mechanical vibration produces a significant effect on the results. We will improve the mechanical stability of the interferometer and try the next experiment in the nearest future.

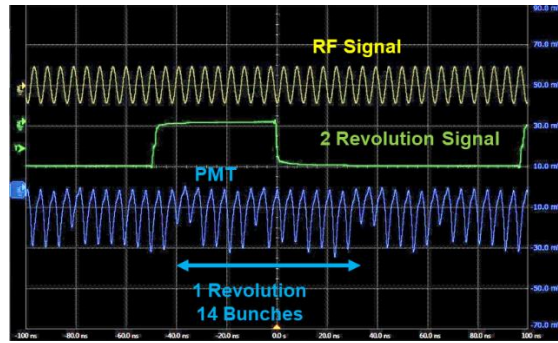


FIGURE 1. Time structure of the bending radiation measured by a photomultiplier at HiSOR-BL8.

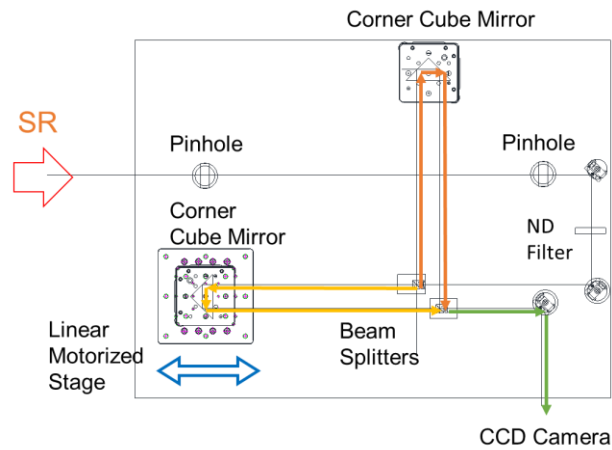


FIGURE 2. Interferometer installed at UVSOR-BL1U.

REFERENCES

1. Y. Miyamoto et al., Opt. Lett. 18, 11 (1993), 900.
2. T. Mitsuhashi and M. Tadano, Proc. EPAC2002 (Paris, 2002), 1936.

Design Study on Laser Focusing System for 90 degree Thomson scattering Gamma-ray source

Hina Kunimune^a, Yasuaki Okano^b, Masahiro Katoh^{a,b}

^a Hiroshima University, 1-3-1 Kagamiyama, Higashi-Hiroshima 739-8526, Japan

^d Institute for Molecular Science, National Institutes of Natural Sciences, 38 Nishigo-Naka, Myodaiji, Okazaki, 444-8585, Japan

Keywords: Laser. Compton scattering, Gamma-ray

Laser Compton scattering is a method to generate high energy photons from electron accelerators. A laser beam is injected onto an electron beam in the accelerators and is scattered via inverse Compton scattering. When the laser photons of around 1eV are scattered by high energy electrons around 1 GeV, gamma-ray photons of MeV energy range are produced. In this parameter range, the scattering in the electron rest frame is well approximated as Thomson scattering. Therefore, in this paper, we call the process laser Thomson scattering (LTS).

The energy of gamma-ray photons can be changed by changing the laser wavelength, the electron energy or the collision angle. The gamma-ray photons are scattered into a narrow cone along the direction of the electron motion. By limiting the scattering angle by using a collimator, one can get quasi-monochromatic gamma-ray beam. Since the polarization of the gamma-rays reflects that of the laser photons, one can control the polarization of the gamma-rays by controlling the laser polarization. LTS gamma-rays possess such remarkable properties which the radioactive isotopes gamma-rays do not.

There are a few operational LTS gamma-ray sources based on electron synchrotrons in the world [1, 2]. In these sources, the laser beam and the electron beam collide each other in a head-on configuration. On the other hand, at UVSOR-BL1U, there is a port to inject the laser beam onto the electron beam with nearly 90-degree collision angle. By utilizing this special experimental condition, the energy tunability by changing the collision angle and ultrashort gamma-ray pulses are successfully demonstrated. Another interesting application of this setup is a micro-focus gamma-ray source, in which the laser beam is focused to a micron size at the colliding point. This is practically possible in the 90-degree configuration but not in the head-on configuration, because we have to place the final focus mirror as close as possible to the colliding point in such a strong focusing. The micro-focus gamma-ray source may be beneficial to improve the resolution of the expanding transmission imaging. Moreover, the high photon density at the colliding point may be useful for investigating non-linear process [3].

In this study, we are developing a laser focusing system for the 90-degree configuration. Considering the possibility of using short pulse laser, we adopt a reflecting optics to avoid the chromatic aberration. For the final focusing mirror, we adopt a parabolic mirror. Before the final focusing, the laser beam should be expanded to realize the micro-focusing. We adopt a beam expander formed with two spherical mirrors. As the first step of the study, we have designed a focus optics assuming to use some commercial optical components. We developed a ray tracing program and simulated the focusing performance. Also, we constructed the optics in the laboratory and observe its performance.

The results are summarized in FIG. 1 and 2. The simulation results indicate that about a half of the photons are focused in an area of the scale of 100 micron, although strong astigmatism is observed, which presumably arises from the off-axis configuration of the spherical mirrors in the expander. The calculation and the measurement are qualitatively consistent with each other. In a previous work, there was proposed a technique to reduce the astigmatism in such an expander configuration by slightly tilting the spherical mirrors [4]. Following this work, we ran a preliminary simulation to see this effect and confirmed it. Based on these results, we are going to design and construct the focus optics for the real experiment.

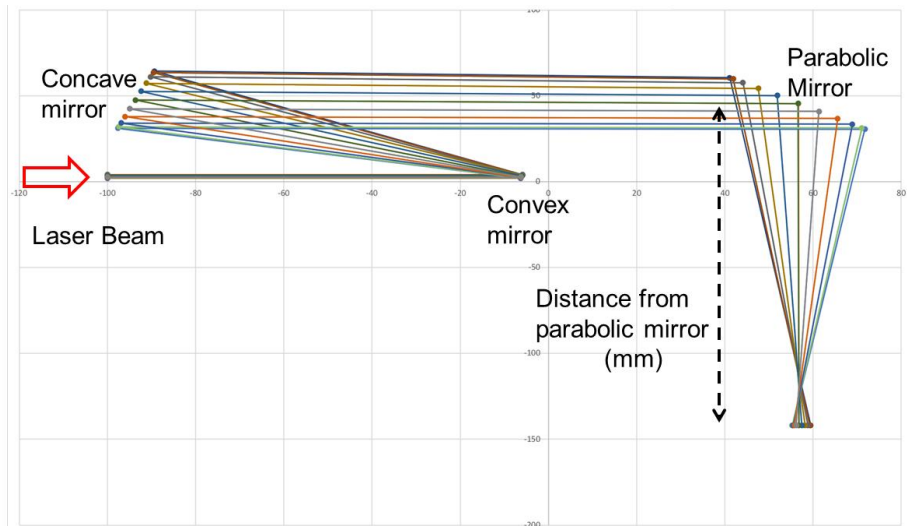


FIGURE 1. Ray tracing of the focusing optics.

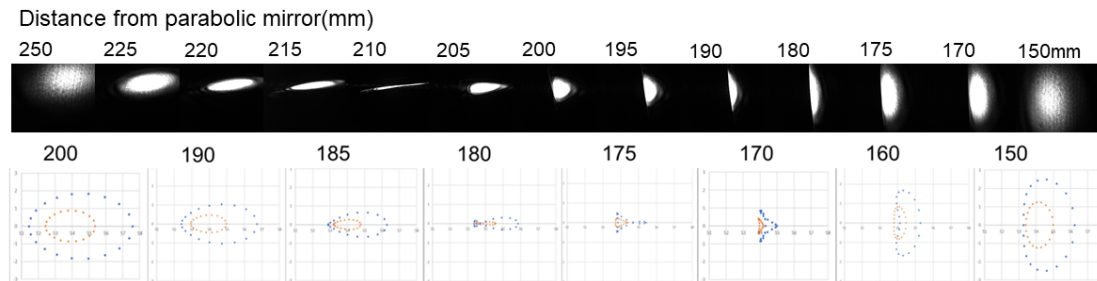


FIGURE 2. Spot diagram and measured laser profiles around the focusing point.

REFERENCES

1. <http://www.tunl.duke.edu/web.tunl.2011a.higs.php>.
2. <http://www.lasti.u-hyogo.ac.jp/NS/facility/bl01/>.
3. Y. Taira, T. Hayakawa & M. Katoh, Sci. Rep. 7, 5018 (2017).
4. P. Hello and C. N. Man, "Design of a low-loss off-axis beam expander", Appl. Opt., 35, 15, 2534 (1996).

Simulation Study on Beam Injection to Compact Synchrotron using Pulse Octupole Magnet

Kakeru Hirata^a, Takashi Ishida^b, Miho Shimada^{c,a}, Masahiro Katoh^{a,d}

^a Hiroshima University, 1-3-1 Kagamiyama, Higashi-Hiroshima 739-8526, Japan

^b Nagoya University, Furo-cho, Chikusa-ku, Nagoya, 464-8601, Japan

^c High Energy Accelerator Research Organization (KEK), 1-1 Oho, Tsukuba, Ibaraki 305-0801 Japan

^d Institute for Molecular Science, National Institutes of Natural Sciences, 38 Nishigo-Naka, Myodaiji, Okazaki, 444-8585, Japan

Keywords: Beam Injection. Storage Ring, Magnet

Beam injection into a storage ring without perturbing the stored beam is a key technology for the top-up operation. In the traditional injection scheme, to reduce the initial amplitude of the betatron oscillation of the injected beam, the orbit of the stored beam is shifted closer to the injected beam at the injection point. This causes movements of the source points of synchrotron radiation, which may be harmful to many applications. In the large facilities, only a small section of the orbit is perturbed and its effect can be minimized for many of the users. In small facilities, however, the perturbation extends over a significant fraction of the ring and, in some cases, it extends over the entire ring. To avoid this, a novel injection scheme was proposed in which the injected beam is deflected by a multipole magnet but the stored beam is not because it is passing through the center of the magnet where the magnetic field is ideally zero [1]. This scheme was tested in a few facilities [2, 3]. Although the injection itself was successful in these previous works, it was recognized that the perturbation to the stored beam is not so small as expected. When a quadrupole magnet was used, the shape of the stored beam was perturbed [2]. When a sextupole magnet was used, the stored beam was kicked by the residual magnetic field at the center which is caused by Eddy current in the magnet itself and in the beam pipe [3]. Considering the results from the previous works, we examine a pulsed octupole magnet, which has more flat field distribution around the center and, in addition, from the symmetry of the configuration, it is expected that the effect of Eddy current is also symmetric around the center and consequently the field is zero at the center.

We have developed a particle tracking simulation code based on the linear equation of motion. The electron trajectory can be calculated using the transfer matrix formalism. The nonlinear effect of the pulse octupole magnet is taken into the calculation under a thin lens approximation. We ran simulations for a model synchrotron whose design is based on a compact synchrotron called NIJI-IV, which has a circumference of about 30 m [4].

The results are shown in FIG. 1 and 2. The former is the electron trajectory for about 10 turns after the injection without a pulsed octupole and the latter with it. The pulse width of the octupole is 1 microsecond and the beam is injected when the field reaches the maximum. The beam circulates in the ring for 5 times before the octupole field comes to be zero. As can be seen in FIG.1, without the octupole, the injected beam oscillates around the reference orbit with a large amplitude and after a few turns, it comes back to the original position, hit the beam pipe and get lost. On the other hand, with the octupole magnet, the amplitude is significantly reduced after a few turns and the injected beam can continue circulating.

In summary, we have shown that there is a possibility to inject the beam into a small synchrotron by using a pulsed octupole magnet. Next step is to carry out more precise calculation as taking into the account the emittance and the energy spread of the injected beam. Also we have to take into the simulation the effect of sextupole magnets which are installed to compensate the chromatic effects. Also, we should design the pulsed octupole magnet.

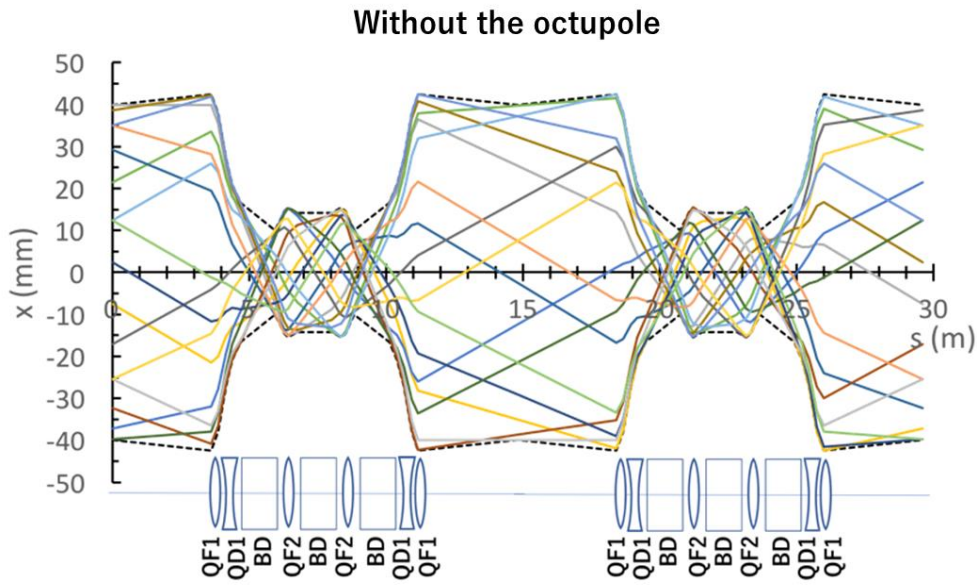


FIGURE 1. Electron trajectory for first 16 turns after the injection without pulse octupole. The dashed lines are the maximum betatron amplitude.

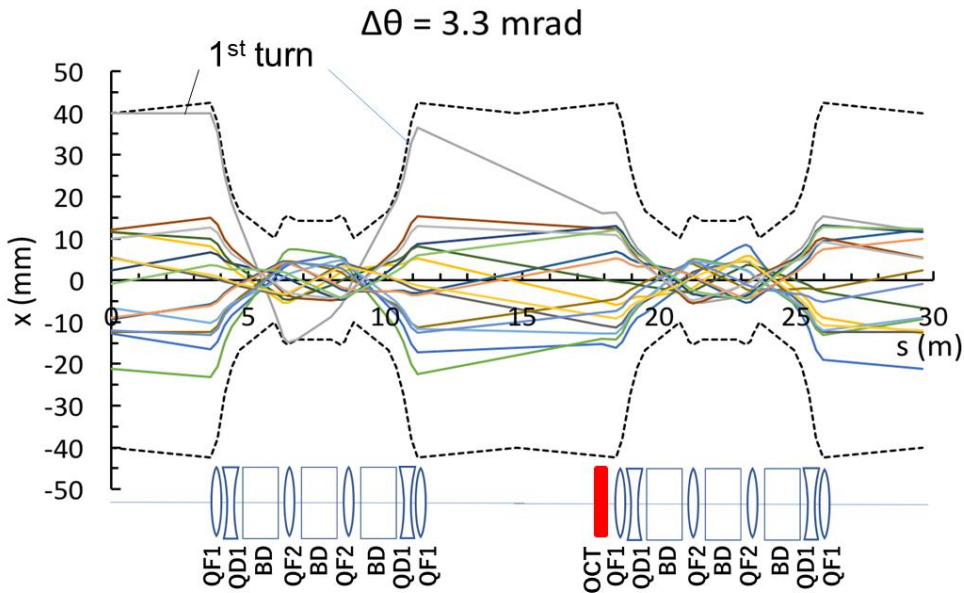


FIGURE 2. Electron trajectory for first 16 turns after the injection with pulse octupole. The position of the octupole is indicated by a red square. The field strength of the octupole is optimized to minimize the betatron amplitude. The trajectory of the first turn is indicated in the figure.

REFERENCES

1. K. Harada, *et. al.*, Phys. Rev. STAB 10 (12) (2007) 123501.
2. H. Takaki, *et. al.*, Phys. Rev. STAB 13 (2010) 020705.
3. N. Yamamoto *et al.*, Nucl. Instr. Meth. Phys. Res. A 767 (2014) 26–33.
4. M. Kawai *et al.*, Nucl. Instr. Meth. Phys. Res. A 318 (1992) 135–141.